Published in final edited form as:
J Biomech. 2010 August 10; 43(11): 2159–2163. doi:10.1016/j.jbiomech.2010.03.048.

Simulation of pulmonary air flow with a subject-specific boundary condition

Youbing Yin[a,b], **Jiwoong Choi**[a,b], **Eric A. Hoffman**[c,d,e], **Merryn H. Tawhai**[f], and **Ching-Long Lin**[a,b,*]

[a] Department of Mechanical and Industrial Engineering, The University of Iowa, Iowa City, Iowa, USA [b] IIHR-Hydroscience and Engineering, The University of Iowa, Iowa City, Iowa, USA [c] Department of Radiology, The University of Iowa, Iowa City, Iowa, USA [d] Department of Biomedical Engineering, The University of Iowa, Iowa City, Iowa, USA [e] Department of Medicine, The University of Iowa, Iowa City, Iowa, USA [f] Auckland Bioengineering Institute, The University of Auckland, Auckland, New Zealand

Abstract

We present a novel image-based technique to estimate a subject-specific boundary condition (BC) for computational fluid dynamics (CFD) simulation of pulmonary air flow. The information of regional ventilation for an individual is derived by registering two computed tomography (CT) lung datasets and then passed to the CT-resolved airways as the flow BC. The CFD simulations show that the proposed method predicts lobar volume changes consistent with direct image-measured metrics, whereas the other two traditional BCs (uniform velocity or uniform pressure) yield lobar volume changes and regional pressure differences inconsistent with observed physiology.

Keywords

Computational fluid dynamics; Pulmonary air flow; Subject-specific boundary condition; Image registration; Finite element

1. Introduction

Computational fluid dynamics (CFD) has become a vital tool in understanding the nature of pulmonary air flow in the human lungs from the large central bronchial airways to the acinar regions. A representative though not exhaustive list of such studies can be found in Choi et al. (2009), Freitas and Schröder (2008), Kumar et al. (2009), Lin and Hoffman (2005), Lin et al. (2007, 2009), Liu et al. (2003), Ma and Lutchen (2009), Stapleton et al. (2000), van Ertbruggen et al. (2005) and Xia et al. (2010). One of its applications is to predict the local deposition of pollutant or therapeutic particles for the purpose of understanding the etiology of lung pathology and for the improvement of drug delivery methods. Since particle deposition is highly dependent on flow characteristics, which, in turn, are dependent on the geometrical configuration of airways and regional ventilation of the lungs, it is desirable to conduct subject-specific CFD with an anatomically realistic airway geometry and a

*Corresponding author. Tel.: +1 319 335 5673; fax: +1 319 335 5669. ching-long-ling@uiowa.edu (C.-L. Lin).

Conflict of interest statement

E.A. Hoffman is a founder and shareholder of VIDA Diagnostics which is commercializing some of the software utilized in this work.

physiologically consistent boundary condition (BC). Due to the complexity of the human tracheobronchial tree, most earlier CFD studies of pulmonary air flow used either the symmetric Weibel (1963) model or the asymmetric Horsfield et al. (1971) model. Although those studies provide some insights into the characteristics of flow in systems of bifurcating tubes, their idealized airway models lack subject-specific geometrical features for assessing an individual's response to inhaled particulates and for better tailoring a treatment plan for the individual. With rapid advances in medical imaging and computational techniques, three-dimensional (3D) realistic airway geometries with major branches derived from high resolution computed tomography (CT) images have recently been used in CFD analyses (Choi et al., 2009; Freitas and Schröder, 2008; Lin et al., 2007, 2009). In addition, one-dimensional (1D) centerline airway models generated from subject-specific lobe configurations, such as by Tawhai et al. (2004), have also been used to investigate gas mixing (Tawhai and Hunter, 2001). However, in most of these studies simple uniform BCs (either uniform velocity, uniform pressure, or uniform flow distribution) were imposed at the ending airway segments, which may limit the accuracy of the results due to the inability to take into consideration the realistic nonuniform ventilation. De Backer et al. (2008) attempted to describe a subject-specific BC by using two different pressure values at the 3D CT-resolved ending segments in the left and right lungs for a steady inspiratory flow. While De Backer et al. (2008) predicted a different flow rate between left and right lungs, their approach is not sufficient to capture the heterogeneity of ventilation inherent to both normal function and pathophysiology of the lung. Recently, Tawhai et al. (2006, 2009), developed a soft-tissue-mechanics-based model for elastic deformation of the compressible lung tissue, in which the local volume change of the peripheral tissue can be used for setting a flow BC for the 1D centerline airway model. And Lin et al. (2009) proposed a multi-scale CFD framework that couples a 3D CT-resolved central airway tree with a 1D centerline airway tree in a physiologically and morphometrically consistent manner: the 1D peripheral airway tree serves as a link between 3D central airway tree and lung parenchyma. With the 1D and 3D coupling framework, a subject-specific BC can be imposed on the 3D central airways via the 1D tree using the information of regional ventilation.

Regional ventilation has been measured using imaging techniques, such as magnetic resonance (MR) (Salerno et al., 2002; van Beek et al., 2004) and xenon CT (Chon et al., 2005, 2007). Currently MR is only partially quantitative because of a limited capability for depiction of anatomic detail. MR is also costly, requiring specialized equipment to hyperpolarize the gas that is used for imaging. Xenon CT can predict a high resolution ventilation map but it requires the use of expensive xenon gas and the associated hardware for controlled gas delivery. Alternatively, regional ventilation can be generated by registering two volumetric CT datasets (Christensen et al., 2007; Guerrero et al., 2006; Reinhardt et al., 2008; Yin et al., 2009a). In contrast to MR or xenon CT, such registration-based analysis of regional ventilation requires only two volumetric datasets of the lung at different levels of inflation and the resulting ventilation map has a high resolution.

The purpose of this work is to describe a technique to estimate a subject-specific BC with two CT lung datasets by means of an image registration method. The derived BC is then applied for CFD simulation of pulmonary air flow and is compared against two traditional BCs.

2. Methods

Fig. 1 shows a flow chart of the entire process. Two CT datasets are acquired at different levels of inflation in the same scanning session and are matched using a mass-preserving image registration (Yin et al., 2009b) to estimate regional ventilation. Meanwhile, a subject-specific 1D centerline airway tree is generated based on the image with larger lung volume

using a volume filling method (Tawhai et al., 2004) that fills lobes with bifurcating tree spanning the entire conducting airways from the ending segments of CT-resolved central airways to terminal bronchioles. The registration-derived regional ventilation map is then associated with the 1D tree to estimate air flows at the approximately 30,000 terminal branches. Terminal airway flows are used to produce the subject-specific flow BC for the 3D CT-resolved central airways by utilizing the connectivity information between the 3D airways and the associated downstream 1D airway branches. The proposed subject-specific BC is then applied to CFD and is compared against two traditional outlet BCs (either uniform velocity or uniform pressure).

In this study, the two 3D CT volumetric datasets were acquired from a normal human subject (a 32-year-old non-Hispanic white male) during breath-holds in a single scanning section. Scan parameters were: 120kV, 100mAs, slice thickness 1.3mm, reconstruction kernel B, field of view 350 mm, rotation speed 0.5s, pitch 1.25. The protocol was approved by the University of Iowa's Institutional Review Board. The subject lay supine and breathed through a mouthpiece during the scanning session. One volumetric dataset was acquired at 85% of VC, referred to hereafter as image I_1, and the other was at 55% of vital capacity (VC), referred to hereafter as image I_2. Each dataset consists of 553 slices with a spacing of 0.6 mm and a reconstruction matrix of 512 × 512 pixels. In-plane pixel spatial resolution is $0.68 \times 0.68 mm^2$. The two datasets were processed using a software package Pulmonary Workstation 2 (PW2: VIDA Diagnostics, Coralville, Iowa) to segment the lungs, lobes and central airways. The segmented airways were further skeletonized to obtain the centerlines of individual branches.

A mass preserving image registration method was used to match the two volumetric CT datasets. This registration method estimates local tissue (parenchyma plus blood) and air fraction within the lung and minimizes the local tissue volume difference. Let $I(x)$ denote the Hounsfield unit (HU) for a voxel at **x**. The tissue and air fraction can be estimated as (Hoffman, 1985; Hoffman et al., 2003)

$$\beta_{air}(\mathbf{x})=\frac{HU_{tissue}-I(\mathbf{x})}{HU_{tissue}-HU_{air}} \quad \text{and} \quad \beta_{tissue}(\mathbf{x})=\frac{I(\mathbf{x})-HU_{air}}{HU_{tissue}-HU_{air}}, \tag{1}$$

where HU_{air} and HU_{tissue} refer to the HUs of air and tissue, respectively. In this work, we used – 1000 for HU_{air} and 55 for HU_{tissue}.

Based on Eq. (1), we can then define the similarity measure as the sum of squared local tissue volume difference (SSTVD):

$$E=\sum_{\mathbf{x}\in\Omega}[V_1(\mathbf{x})\beta_{tissue1}(\mathbf{x})-V_2(T(\mathbf{x}))\beta_{tissue2}(T(\mathbf{x}))]^2, \tag{2}$$

where $T(\mathbf{x})$ is the transform function to be optimized and a cubic B-spline model is adopted in this work. V_1 and V_2 are total volumes of corresponding regions in the two images, respectively, and V_2 can be calculated from the Jacobian value J_T of the deformation as $V_2 = J_T V_1$. For complete details, please refer to Yin et al. (2009b). We have previously validated this method based on six pairs of volumetric CT datasets and it has been shown to be effective at registering intra-subject lung CT datasets (Ding et al., 2009;Yin et al., 2009b).

Once the image registration is performed, we can further calculate regional ventilation, which is also referred to as the local air volume difference in this work. The local air volume

difference is jointly estimated from changes in local air fraction along with the registration-derived local Jacobian value (Yin et al., 2009a). The regional ventilation map describes local air volume changes between the two volumetric datasets. Thus, it can be used to provide a subject-specific BC for the 3D central airways in a 3D and 1D coupling framework (Lin et al., 2009).

The current 1D airway tree was generated using a previously proposed volume filling method. The volume filling method takes the lobes as “boundary conditions” and the skeleton of the 3D CT-resolved central airways as “initial conditions” (Tawhai et al., 2004). To date, this is the only published method that has been demonstrated to produce human airway models consistent with morphometric measurements. The volume filling method generates the 1D centerline airway model based on the image close to TLC with the assumption that the pulmonary acini are uniformly distributed. A set of seed points is uniformly distributed in the lung with the number approximately equal to the expected number of terminal bronchioles (30,000). Each terminal branch supplies a unique point that represents the center of an acinus, i.e. a parenchymal unit. The air flow at each terminal bronchiole can then be calculated as the sum of registration-derived regional ventilation of all voxels in that unit. By mass conservation the air flow at an ending segment of the CT-resolved 3D central airways can be determined by summing the air flows of terminal bronchioles with the connectivity information between the 3D airway and the associated downstream 1D airway branches.

Simulations of inspiratory flows using the proposed BC and two conventional uniform BCs were performed in this study. Large eddy simulation (LES) was adopted to capture transitional and turbulent flow. The governing equations consist of the filtered continuity equation and Navier–Stokes equations for incompressible flow:

$$\frac{\partial \overline{u}_j}{\partial x_j}=0, \tag{3}$$

$$\frac{\partial \overline{u}_i}{\partial t}+\overline{u}_j\frac{\partial \overline{u}_i}{\partial x_j}=-\frac{1}{\rho}\frac{\partial \overline{p}}{\partial x_i}+\frac{\partial}{\partial x_j}\left[(\nu+\nu_T)\frac{\partial \overline{u}_i}{\partial x_j}\right], \tag{4}$$

where u_i, p, ρ, ν, and ν_T are the i th component of velocity, pressure, density, kinematic viscosity, and subgrid-scale eddy viscosity, respectively. The density and the kinematic viscosity of the air are 1.2kg/m^3 and 1.7×10^{-5} m^2/s, respectively. The overbar denotes resolved quantities. The eddy-viscosity subgrid-scale model proposed by Vreman (2004) was used to account for the transitional and anisotropic flow characteristics. A fractional four-step and characteristic Galerkin method based finite element scheme was employed in solving Eqs. (3) and (4) (Lin et al., 2005). An unstructured mesh with 899,465 nodes and 4,644,447 tetrahedral elements was generated for the CT-resolved upper and central airways. The whole computational domain was divided into 256 partitions and the simulation was conducted on the Lonestar cluster at the Texas Advanced Computing Center. The time step was set to 2.0×10^{-5} s, resulting in an average Courant–Friedrichs–Lewy (CFL) number of about 0.044. Further details of the 3D fluid solver including validation can be found in Lin et al. (2007) and Choi et al. (2009), where LES solutions were compared with those of refined LES and direct numerical simulations. A flow rate of 0.342 L/s at the peak inspiration was imposed at the mouthpiece inlet, resulting in a Reynolds number of 1380 in the trachea. The outlet BCs at the ending airway segments were set with the

proposed subject-specific BC (case 1), uniform velocity BC (case 2) and uniform pressure BC (case 3), respectively. The reference pressure was selected at the tracheal inlet.

3. Results

Registration-derived regional ventilation was validated by comparing with measured global values: (1) the average Jacobian value and (2) the total air volume difference. The measured average Jacobian value is defined as the ratio of the total lung volume of image I_2 to that of image I_1, where the total lung volumes for images I_1 and I_2 are 7.60 L and 6.09 L, respectively. The measured total air volumes can be calculated from the total lung volume and the average air fraction, where the average air fraction is estimated from average HU inside the lung with Eq. (1). For the images I_1 and I_2 used in this study, the measured total air volumes are 6.72 and 5.20 L, respectively. Thus, the measured total air volume difference is 1.52 L between the two images. In contrast to the measured values, the registration-derived average Jacobian value is calculated from local Jacobian values in the lungs and the registration-derived total air volume difference is the sum of local air volume difference of all voxels in the lungs. Table 1 presents the comparison between the measured values and the registration-derived values. It is clear that the registration-derived average Jacobian value matches well with the measured one and the registration-derived total air volume difference is also close to the measured value with a small error of 2.6%.

Fig. 2(a) shows the surface geometries of the lobes, CT-resolved upper and central airways for image I_1. These surface geometries are obtained by converting the segmentation into surface meshes with a Marching Cubes algorithm (Lorensen and Cline, 1987) and further smoothing the meshes using a without-shrinkage smooth technique (Taubin, 1995). Fig. 2(b) shows the generated 1D centerline airway tree. The 3D CT-resolved upper and central airways with the central airway skeleton are also shown in Fig. 2(b). The lobes and lobar airway trees are shown in different colors: green for the left upper lobe (LUL), red for the left lower lobe (LLL), cyan for the right upper lobe (RUL), blue for the right middle lobe (RML) and purple for the right lower lobe (RLL).

Fig. 3 compares the distributions of outlet velocity and static pressure for the three cases. The distributions in Fig. 3(a) for the proposed BC are more heterogeneous than those of the uniform velocity BC in Fig. 3(b) and the uniform pressure BC in Fig. 3(c). In particular, the proposed BC predicts much greater pressure drop at the airways in the LLL and the RLL shown in Fig. 3(a). In contrast, the uniform velocity BC yields greater pressure drop in the RML than others, whereas the uniform pressure BC enforces the same pressure drop in all five lobes.

Quantitative comparisons of lobar distribution of air flow are presented in Fig. 4. The proposed method results in larger deviation between lobes, reflecting the nature of heterogeneity of ventilation in the human lung. The measured values (the lobar difference of air content) are also shown. The lobar distributions predicted by the proposed method match well with these measured values with an overall relative error of 4.79%, seen from Table 2. The large relative error for RML is due to the small measured value for that lobe (0.052). However, the uniform outlet velocity and uniform outlet pressure methods yield errors of 43.42% and 27.08%, respectively. The uniform velocity BC results in over-prediction (more than twice) of the ventilation to the RML, yielding a greater pressure drop in the RML shown in Fig. 3(b). Both uniform pressure and uniform velocity BCs under-predict the ventilation to the two lower lobes LLL and RLL.

4. Discussions

In conclusion, we have described a technique to estimate a subject-specific BC for CFD simulation of pulmonary air flow. In contrast to the idealized symmetric airway models, the real human airways are asymmetric and BCs most certainly play an important role in determining the regional distributions of basic flow properties. Advantages of the current BC have been investigated by comparing the CFD results using the proposed subject-specific BC against two traditional BCs (uniform outlet velocity and uniform outlet pressure). The results showed that the lobar and regional distributions of pressure and flow rates in the bronchioles were noticeably affected by the outlet BCs. As compared with the measurement data, the proposed method yielded physiologically reasonable regional distribution of flow, which was not accomplished by the other two BC methods.

To our knowledge, this work is the first attempt to provide realistic BCs for CFD simulations based upon image registration. The method proposed here uses two volumetric images of the lung acquired at different lung volumes and produces BCs that are specific to the subject and to their change in regional lung volume. This method can be extended to match multiple lung volumes acquired between TLC and FRC in the same scanning session, thus providing a way to develop a computational lung model with realistic time-varying BCs in a breathing period. In addition, the proposed method would benefit from further validation of the registration-derived regional ventilation, such as comparing with the measurements from xenon CT, or hyperpolarize ^{3}He MR (Chon et al., 2005, 2007; Fuld et al., 2008). The validated technique would then be applicable to study pulmonary airflow in subjects with lung diseases that affects ventilation distribution, such as asthma or chronic obstructive pulmonary disease. In these cases, a next step will be to adjust the airway model based upon additional image-based information related to regional tissue destruction (Hogg et al., 2009).

Acknowledgments

This work was supported in part by NIH Grant nos. R01-HL-064368, R01-EB-005823, S10-RR-022421, R01-HL-094315, and a University of Iowa CTSA NIH/NCRR Grant no. 1UL1RR024979. The authors also thank TeraGrid via the Texas Advanced Computing Center for allocating computer time for CFD simulations.

References

Choi J, Tawhai MH, Hoffman EA, Lin CL. On intra- and intersubject variabilities of airflow in the human lungs. Physics of Fluids 2009;21 (10):101901. [PubMed: 19901999]

Chon D, Beck KC, Simon BA, Shikata H, Saba OI, Hoffman EA. Effect of low-xenon and krypton supplementation on signal/noise of regional CT-based ventilation measurements. Journal of Applied Physiology 2007;102 (4):1535–1544. [PubMed: 17122371]

Chon D, Simon BA, Beck KC, Shikata H, Saba OI, Won C, Hoffman EA. Differences in regional wash-in and wash-out time constants for xenon-CT ventilation studies. Respiratory Physiology & Neurobiology 2005;148 (1–2):65–83. [PubMed: 16061426]

Christensen GE, Song JH, Lu W, Naqa IE, Low DA. Tracking lung tissue motion and expansion/compression with inverse consistent image registration and spirometry. Medical Physics 2007;34 (6):2155–2163. [PubMed: 17654918]

De Backer JW, Vos W, Gorle C, Germonpre P, Partoens B, Wuyts FL, Parizel PM, De Backer M. Flow analyses in the lower airways: patient-specific model and boundary conditions. Medical Engineering & Physics 2008;30 (7):872–879. [PubMed: 18096425]

Ding, K.; Yin, Y.; Cao, K.; Christensen, GE.; Lin, C-L.; Hoffman, EA.; Reinhardt, JM. Evaluation of lobar biomechanics during respiration using image registration. Proceedings of the 12th International Conference on Medical Image Computing and Computer-Assisted Intervention; London, UK. 2009. p. 739-746.

Freitas RK, Schröder W. Numerical investigation of the three-dimensional flow in a human lung model. Journal of Biomechanics 2008;41 (11):2446–2457. [PubMed: 18614172]

Fuld MK, Easley RB, Saba O, Chon D, Reinhardt JM, Hoffman EA, Simon BA. CT measured regional specific volume change reflects regional specific ventilation in supine sheep. Journal of Applied Physiology 2008;104 (4):1177–1184. [PubMed: 18258804]

Guerrero T, Sanders K, Castillo E, Zhang Y, Bidaut L, Pan T, Komaki R. Dynamic ventilation imaging from four-dimensional computed tomography. Physics in Medicine and Biology 2006;51:777–791. [PubMed: 16467578]

Hoffman EA. Effect of body orientation on regional lung expansion: a computed tomographic approach. Journal of Applied Physiology 1985;59:468–480. [PubMed: 4030599]

Hoffman EA, Reinhardt JM, Sonka M, Simon OS, Chon D, Samrah S, Shikata H, Tschirren J, Palagyi K, Beck KC, McLennan G. Characterization of the interstitial lung diseases via density-based and texture-based analysis of computed tomography images of lung structure and function. Academic Radiology 2003;10 (10):1104–1118. [PubMed: 14587629]

Hogg JC, McDonough JE, Gosselink JV, Hayashi S. What drives the peripheral lung-remodeling process in chronic obstructive pulmonary disease? Proceedings of the American Thoracic Society 2009;6(8):668–672. [PubMed: 20008873]

Horsfield K, Dart G, Olson D, Filley G, Cumming G. Models of the human bronchial tree. Journal of Applied Physiology 1971;31 (2):207–217. [PubMed: 5558242]

Kumar H, Tawhai MH, Hoffman EA, Lin CL. The effects of geometry on airflow in the acinar region of the human lung. Journal of Biomechanics 2009;42 (11):1635–1642. [PubMed: 19482288]

Lin, C-L.; Hoffman, EA. SPIE Medical Imaging '05. Vol. 5746. SPIE; Bellingham, WA: 2005. A numerical study of gas transport in human lung models; p. 92-100.

Lin CL, Lee H, Lee T, Weber LJ. A level set characteristic galerkin finite element method for free surface flows. International Journal for Numerical Methods in Fluids 2005;49 (5):521–548.

Lin CL, Tawhai MH, McLennan G, Hoffman EA. Characteristics of the turbulent laryngeal jet and its effect on airflow in the human intra-thoracic airways. Respiratory Physiology & Neurobiology 2007;157 (2–3):295–309. [PubMed: 17360247]

Lin CL, Tawhai MH, McLennan G, Hoffman EA. Multiscale simulation of gas flow in subject-specific models of the human lung. IEEE Engineering in Medicine and Biology Magazine 2009;28 (3):25–33. [PubMed: 19457731]

Liu Y, So R, Zhang C. Modeling the bifurcating flow in an asymmetric human lung airway. Journal of Biomechanics 2003;36 (7):951–959. [PubMed: 12757804]

Lorensen WE, Cline HE. Marching cubes: a high resolution 3D surface construction algorithm. Computer Graphics 1987;21 (4):163–169.

Ma B, Lutchen K. CFD simulation of aerosol deposition in an anatomically based human large-medium airway model. Annals of Biomedical Engineering 2009;37:271–285. [PubMed: 19082892]

Reinhardt JM, Ding K, Cao K, Christensen GE, Hoffman EA, Bodas SV. Registration-based estimates of local lung tissue expansion compared to xenon CT measures of specific ventilation. Medical Image Analysis 2008;12 (6):752–763. [PubMed: 18501665]

Salerno M, de Lange E, Altes T, Truwit J, Brookeman J, Mugler J. Emphysema: hyperpolarized helium 3 diffusion MR imaging of the lungs compared with spirometric indexes—initial experience. Radiology 2002;222 (1):252–260. [PubMed: 11756734]

Stapleton K, Guentsch E, Hoskinson M, Finlay W. On the suitability of k–ε turbulence modeling for aerosol deposition in the mouth and throat: a comparison with experiment. Journal of Aerosol Science 2000;31 (6):739–749.

Taubin, G. Curve and surface smoothing without shrinkage. Proceedings of the Fifth International Conference on Computer Vision '95; Washington, DC. 1995. p. 852-857.

Tawhai MH, Hunter P, Tschirren J, Reinhardt JM, McLennan G, Hoffman EA. CT-based geometry analysis and finite element models of the human and ovine bronchial tree. Journal of Applied Physiology 2004;97 (6):2310–2321. [PubMed: 15322064]

Tawhai MH, Hunter PJ. Multibreath washout analysis: modelling the influence of conducting airway asymmetry. Respiration Physiology 2001;127 (2–3):249–258. [PubMed: 11504594]

Tawhai MH, Nash MP, Hoffman EA. An imaging-based computational approach to model ventilation distribution and soft-tissue deformation in the ovine lung. Academic Radiology 2006;13 (1):113–120. [PubMed: 16399039]

Tawhai MH, Nash MP, Lin CL, Hoffman EA. Supine and prone differences in regional lung density and pleural pressure gradients in the human lung with constant shape. Journal of Applied Physiology 2009;107 (3):912–920. [PubMed: 19589959]

van Beek EJR, Wild JM, Kauczor HU, Schreiber W, Mugler JP, de Lange EE. Functional MRI of the lung using hyperpolarized 3-helium gas. Journal of Magnetic Resonance Imaging 2004;20 (4): 540–554. [PubMed: 15390146]

van Ertbruggen C, Hirsch C, Paiva M. Anatomically based three-dimensional model of airways to simulate flow and particle transport using computational fluid dynamics. Journal of Applied Physiology 2005;98 (3):970–980. [PubMed: 15501925]

Vreman A. An eddy-viscosity subgrid-scale model for turbulent shear flow: algebraic theory and applications. Physics of Fluids 2004;16:3670.

Weibel, ER. Morphometry of the Human Lung. Academic; New York: 1963.

Xia G, Tawhai MH, Hoffman EA, Lin CL. Airway wall stiffening increases peak wall shear stress: a fluid-structure interaction study in rigid and compliant airways. Annals of Biomedical Engineering 2010;38 (5):1836–1853. [PubMed: 20162357]

Yin, Y.; Hoffman, EA.; Lin, C-L. SPIE Medical Imaging ’09. Vol. 7262. SPIE; 2009a. Local tissue-weight-based nonrigid registration of lung images with application to regional ventilation; p. 72620C

Yin Y, Hoffman EA, Lin CL. Mass preserving nonrigid registration of CT lung images using cubic B-spline. Medical Physics 2009b;36 (9):4213–4222. [PubMed: 19810495]

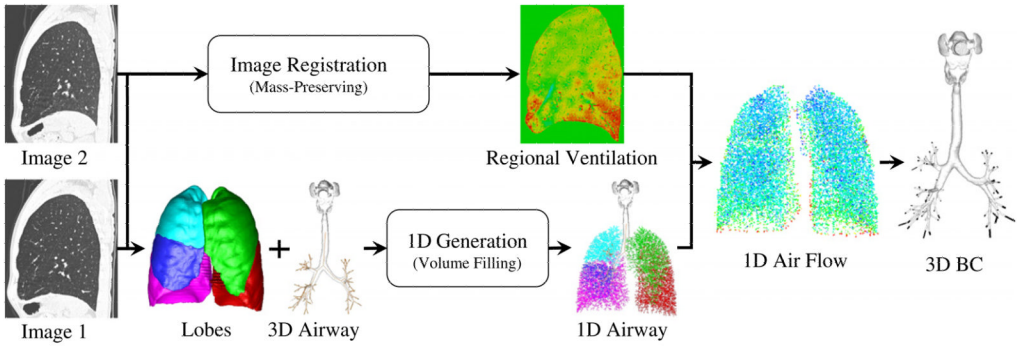

Fig. 1.
A flow chart of the entire process.

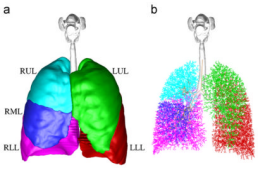

Fig. 2.

(a) Surface geometries of the lobes (LUL: left upper lobe; LLL: left lower lobe; RUL: right upper lobe; RML: right middle lobe; and RLL: right lower lobe), CT-resolved upper and central airways for image I_1; (b) combination of generated 1D centerline airway tree with the 3D CT-resolved upper airway, central airway tree and central airway skeleton.

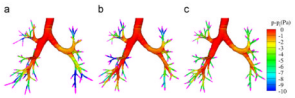

Fig. 3.

Outlet velocity vectors (pink) and pressure contours for the three different outlet BCs: (a) proposed; (b) uniform velocity; and (c) uniform pressure. (For interpretation of the references to color in this figure legend, the reader is referred to the web version of this article.)

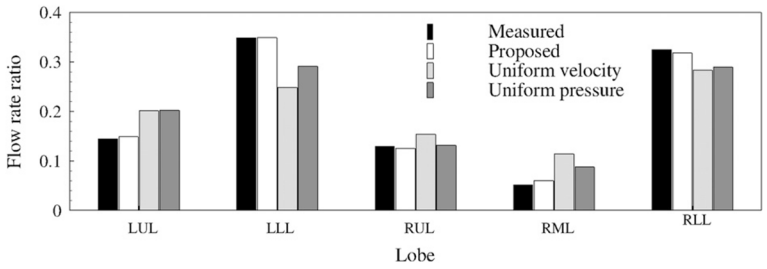

Fig. 4.
Lobar distribution of flow rate ratio for the three cases with different outlet BCs.

Table 1

Comparison between measured and registration-derived values for average Jacobian value and total air volume difference.

	Average Jacobian value	Total air volume difference (L)
Measured	0.80	1.52
Registration-derived	0.80	1.56
Error percentage (%)	0.0	2.6

Table 2

Relative errors of the lobar distributions of flow rate ratio for the three outlet BCs against measured values.

	Proposed (%)	Uniform velocity (%)	Uniform pressure (%)
LUL	3.13	38.61	39.19
LLL	0.09	28.81	16.56
RUL	3.86	18.99	1.00
RML	14.73	117.93	67.69
RLL	2.12	12.76	10.94
Overall	4.79	43.42	27.08